Flexible Battery-Less Bioelectronic Implants: Wireless Powering and Manipulation by Near-Infrared Light

Hongzhong Liu, Tingting Zhao, Weitao Jiang, Rui Jia, Dong Niu, Guanglin Qiu, Lin Fan, Xin Li, Weihua Liu, Bangdao Chen, Yongsheng Shi, Lei Yin, and Bingheng Lu*

Bioelectronics, which can provide electrical impulses to precisely modulate the body's neural circuits, spark great interests of industry and academia. Yet the technologies to power and manipulate these devices, such as wireless powering and remote manipulation, remain challenging. Here, by investigating the pyroelectric performances of poly(vinylidene difluoride) (PVDF) and its remote-manipulation ability under near-infrared-ray (nIR) irradiation, a flexible battery-less implantable device is proposed, constructed by laminated graphene–PVDF–graphene sandwiches, which can be wirelessly powered and supply regulatable electrical pulses for nerve stimulation by nIR irradiation. The flexible and compact device (20 mm × 20 mm in area, 0.2 mm in thickness) can generate electrical pulses with controllable amplitude and width, and shows an excellent ability to stimulate nerves, i.e., sciatic nerve of a frog and a rat heart, by remote control. The flexible and remote-manipulative battery-less device should find uses in the design and fabrication of bioelectronics-related applications.

1. Introduction

Bioelectronics, a recently coined term that broadly encompasses all bioelectronic implants, which could send an electrical pulse to a major nerve to alter the commands an organ receives, and thereby control its function, are more precise than conventional pharmaceuticals, and spark great interests of industry and academia.[1,2] Bioelectronics are now available for a wide range of disorders, including retinal and cochlear implants, deep brain stimulators for epilepsy and Parkinson's disease, pacemakers and brain-machine interfaces, among a host of others. In many cases, however, the longevity of the whole bioelectronics implants is determined by the battery lifespan, which must be surgically replaced if their batteries are dead. Surgical procedures to replace the depleted batteries of implantable devices expose patients to health risks, heightened morbidity, and even potential mortality. The health burden and costs are substantial.[3] In addition, integrated batteries often occupy >90% of the devices volume,[4] which calls for a miniaturizing batteries. Although advances in battery technology have led to substantial reductions in overall sizes and increases in storage capacities, operational lifetimes remain limited, rarely exceeding a few years for implants. So a miniature and "battery-less" power supply is greatly desired for bioelectronics. Besides, for bioelectronics intervention in body, their flexibility and the stimuli controllability are also the greatest challenges. The flexibility and softness determine if conformal contact with tissue can be formed, which is responsible for minimal inflammatory response and stable indwelling for a long period.[5,6] Precise modulation is also important for bioelectronics (e.g., neurostimulation): in mice, stimulation of cells in the neural circuit for hunger with a 20 Hz waveform causes voracious eating within minutes, and food intake can be more finely modulated by the number and frequency of stimulation potentials in specific cells.[1,7]

A conceptually interesting means for battery-less power is by energy harvesting directly from natural processes of the body,[3,8] which can extract power from chemical, mechanical, and thermal processes in the human body.[9,10] Examples include natural vibrations of the heart, lung, and diaphragm,[3] use of glucose oxidation,[10] and electric potentials of the inner ear.[11] Although such phenomena provide promising opportunities for power supply to implantable devices, the power densities of such systems are generally quite low to power miniature implants,[4] and the controllability of the stimuli, such as magnitude, frequency, and timeliness, is relatively weak.

Alternatively, energy can be also transferred from an external source by wireless transport. The most investigated wireless

Prof. H. Liu, T. Zhao, Prof. W. Jiang, D. Niu, Dr. B. Chen, Dr. Y. Shi, Dr. L. Yin, Prof. B. Lu
State Key Laboratory for Manufacturing Systems Engineering
Xi'an Jiaotong University
Xi'an 710049, P. R. China
E-mail: wtjiang@mail.xjtu.edu.cn
R. Jia
Department of Neurology
First Affiliated Hospital of Xi'an Jiaotong University
Xi'an 710061, P. R. China
G. Qiu, Prof. L. Fan
Department of General Surgery
First Affiliated Hospital of Xi'an Jiaotong University
Xi'an 710061, P. R. China
Prof. X. Li, Prof. W. Liu
Department of Microelectronics
Xi'an Jiaotong University
Xi'an 710049, P. R. China

DOI: 10.1002/adfm.201502752

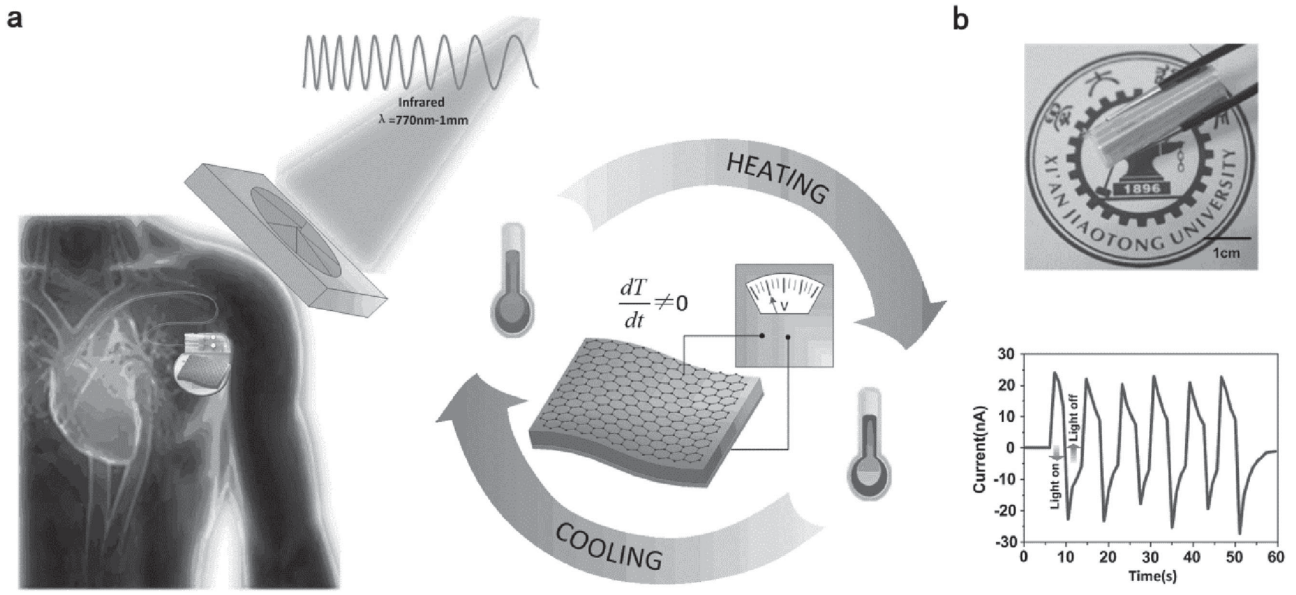

Figure 1. Scheme of a compact, flexible battery-less device for wireless powering and nerve stimulators which can be remotely manipulated by nIR irradiation. a) Flexible battery-less bioelectronics set-up. b) Photograph of a laminated sample.

power is based on electromagnetic coupling, in which the powering transfer is by a coil inside the implant harvesting the energy from external magnetic field,[12,13] including two wireless modalities terms (far-field[14,15] and near field[16]. In order to further enhance the wireless powering properties, Ho et al.[13] developed an antenna, worn on the skin like a patch, that focus electromagnetic radiation in the direction of an implanted device. Although its well controllability, the miniaturization, and flexibility remain the key challenges for the wireless power by electromagnetic coupling.[4]

Besides the wireless power transport by electromagnetic coupling, near infrared ray (nIR), 760–1500 nm in wavelength and known for its heating and medical physical therapy effects,[17,18] provides an alternative wireless power, which can penetrate into human tissue about 4–10 cm.[19] In this paper, we propose a nIR-driven wireless-powering device composed of poly(vinylidene difluoride) (PVDF) microbelts (**Figure 1**). Besides its lightweight, mechanical flexibility,[20] and biocompatibility,[21] which are particularly interesting for wearable or implantable devices,[22] PVDF also shows strong pyroelectric effect (above 40 μC m^{-2} K^{-1} in pyroelectric coefficient), strong absorption of infrared radiation as well as their demonstrated compatibility with graphene.[23] By controllable nIR flashing remotely, the wireless-power device can absorb light and induce temperature fluctuation of PVDF, thus generate voltage/current pulse, which can be used for biological stimulation or batteries charging. Moreover, in order to enhance its electric properties while reducing the device temperature to avoid damage to intervening and surrounding normal tissue, we further developed a compact laminated wireless-power device, in which each cell is composed of graphene–PVDF–graphene sandwich, by employing the well transparency, conductivity, and flexibility of graphene.[24] The constructed laminated wireless-powering device, which is compact (20 mm × 20 mm × 0.2 mm) and flexible, can generate voltage and current up to 2 V and 200 nA, response to nIR remote irradiation with well controllability. The generated electric energy can be effectively stored to light up an array of commercial light-emitting diode (LED). More interestingly, the generated electric pulse, which can be fully controlled by nIR irradiation intensity and frequency, can be directly applied for nerve stimulation, such as sciatic nerve of a frog, and the heart of a live rat, indicating that the proposed battery-less device can be a candidate for bioelectronics.

2. Results and Discussion

2.1. Scheme of Flexible Battery-Less Bioelectronic Implants

A pyroelectric generator (PG) was illuminated periodically on the top by infrared light through a controllable shutter (as Figure 1a shows), which induces a controllable temperature fluctuation and generates voltage/current pulses. The PG was fabricated by coating electrodes on both sides of a pyroelectric element, i.e., PVDF film. Compared to around 90% reflection of Al film, graphene allows more than 90% nIR light to pass (Supporting Information, Figure S1), thus can be preferred as top electrode. We first constructed graphene–PVDF–Al sandwiched PG, in which the Al electrode on the back side can be also considered as a reflector to increase the light absorption. The absorption spectra of graphene–PVDF–Al PG and Al–PVDF–Al PG were measured, respectively. Compared to the PG with Al as top electrode, the PG with graphene as top electrode shows stronger nIR absorption in range of 760–1500 nm (Supporting Information, Figure S2), thus would induce considerable enhancement of temperature-change rate when irradiation, so does for the output voltage/current (Supporting Information, Figure S3). Detailed fabrication process is demonstrated in the Experimental Section.

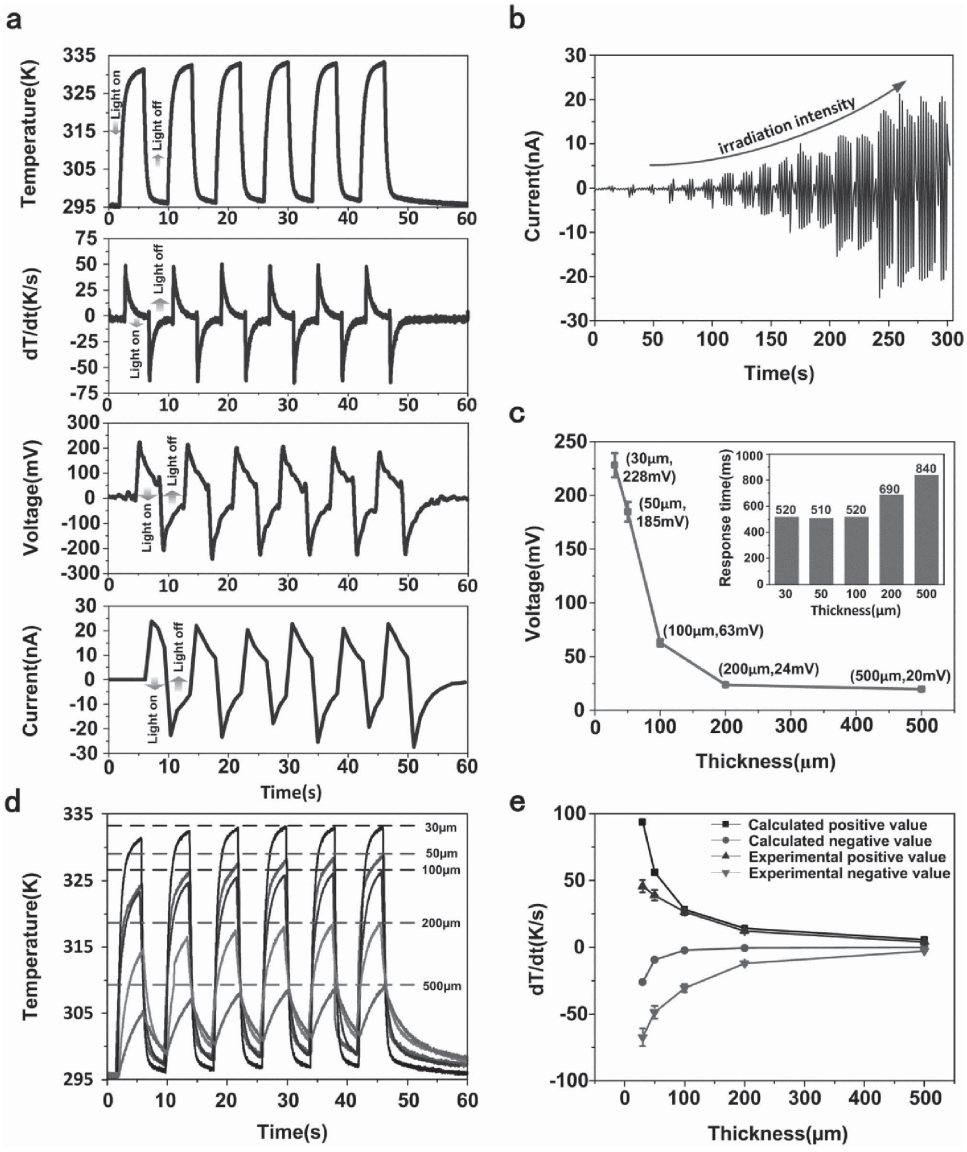

Figure 2. Characterization of the battery-less PG device. a) Cyclic changes in the temperature, temperature-change rate, and the output open-circuit voltage and short-circuit current, response to a controllable nIR irradiation. b,c) Indication of the factors which affect device output. b) Irradiation intensity dependence of the short-circuit current. c) PVDF thickness dependence of open-circuit voltage and the response time. d) The PVDF thickness dependence of temperature variation at cyclic nIR on/off. e) The calculated and experimental temperature-change rate at the time of nIR on and off. The temperature-change rate is inversely proportional to PVDF thickness. According to the pyroelectric equation, the output current/voltage of PG is proportional to the temperature-change rate, so, the output current/voltage would drop rapidly as the PVDF thickness increases.

2.2. Electrical Characterization of the Battery-Less Device

It is well known that, temporary voltage/current can be generated when a pyroelectric material (e.g., PVDF) is heated or cooled. For the graphene–PVDF–Al sandwich, when nIR light controllably flashes on the surface, the temperature of PVDF rises when light is on, and drops when light is off, thus generates temporary voltage/current at the time of light on/off. **Figure 2**a illustrates the temperature fluctuation and induced voltage/current output when nIR flashes on the device with 30 μm thick PVDF. A sharp positive voltage/current pulse (≈228 mV; 25 nA) was observed when the irradiation is on, response to the temperature rises from 296 to 334 K, and a negative pulse when the light is off, response to the temperature drops from 334 to 296 K, at the temperature-change rate of 63 K s^{-1} in both cases. When the device reversely connecting to the measurement system, opposite signals with the same amplitudes were also observed (Supporting Information, Figure S4), suggesting that the voltage/current outputs were generated by the PG.

According to pyroelectricity theory, the pyroelectric current I_p can be described by[25]

$$I_p = p \times A \times \frac{dT}{dt} \quad (1)$$

where p is pyroelectric coefficient (unit: μC m^{-2} K^{-1}), A is the effective area (unit: m^{-2}), and dT/dt is the temperature-change rate (unit: K s^{-1}). The pyroelectric coefficient of PVDF is about 40 μC m^{-2} K^{-1}, which is much larger than those of the reported ZnO and $KNbO_3$.[26,27]

The short-circuit current of the PG is gradually enhanced (Figure 2b) when the irradiation light intensity elevates from 0.21 to 2.95 W cm^{-2} which induces the rise of temperature and its changing rate. According to Equation (1), the current is determined by the temperature-change rate which is roughly linear dependent on the irradiation intensity (Supporting Information, Figure S5). It is also observed that the output voltage/current is also determined by the thickness of the adopted PVDF, the voltage drops from 228 to 20 mV, as the PVDF thickness ranges from 30 to 500 μm (Figure 2c). The PVDF thickness dependence of the output voltage can be attributed to the response of the temperature-change rate, in which the temperature-change for thinner film is more sensible to the external stimulation (light on/off). To reveal the PVDF thickness dependence of the temperature-change rate, the temperature variations for PG devices with different PVDF thickness were measured (Figure 2d). When a pyroelectric material is exposed to radiation of power density (W) for a period (Δt), radiation energy is absorbed and induces temperature elevation (ΔT). For thin film, it is assumed that all of the energy absorbed can be rapidly distributed through the pyroelectric element volume, resulting in a uniform temperature distribution simultaneously. In this case, to simplify the model, heat loss from the pyroelectric are neglected. The temperature elevation can be described by[28]

$$\Delta T = \frac{W \times \Delta t}{C_E \times \delta} \tag{2}$$

Where δ is the pyroelectric thickness (unit: m), and C_E is the volume specific heat (unit: J m^{-3} K^{-1}). It is obvious that the temperature elevation ΔT is inversely proportional to PVDF thickness under the same power density and irradiation time. The temperature-change rate (at the time of light on) can be given by

$$\left.\frac{dT}{dt}\right|_{nIR\text{-}ON} = \frac{W}{C_E \times \delta} \tag{3}$$

Due to $B_i = hl/\lambda \le 0.1$, where h is convective heat transfer coefficient (unit: W m^{-2} K^{-1}), l is half of thickness δ, λ is thermal conductivity (unit: W m^{-1} K^{-1}), according to the 0D unsteady heat conduction differential equations, the temperature-change rate at the time of light off can be described as

$$\left.\frac{dT}{dt}\right|_{nIR\text{-}OFF} = -\frac{h \times A}{C_E \times V} \times (T - T_{air}) \tag{4}$$

Where A is surface area of sample (unit: m^2), V is volume of sample (unit: m^3), T and T_{air} (unit: K) are the temperature of sample and air, respectively. At the time of nIR off after exposure to radiation for a period (Δt)

$$T - T_{air} = \frac{W \times \Delta t}{C_E \times \delta} \tag{5}$$

According to Equations (4) and (5), the temperature-change rate at the time of nIR off can be given by

$$\left.\frac{dT}{dt}\right|_{nIR\text{-}OFF} = -\frac{h \times A \times W \times \Delta t}{C_E^2 \times V \times \delta} \tag{6}$$

So, the temperature-change rate at the time of nIR irradiation on and off can be calculated, respectively (Figure 2e). The physical parameters of PVDF can be found in Table S1 (Supporting Information). It is found that the calculated temperature-change rate generally agrees with experimental values (Supporting Information, Figure S6) in tendency. The deviation between calculated and experimental values could be attributed to the model simplification. For positive temperature-change rate, experimental values are lower than calculated values, which may attribute to the neglected heat loss in the temperature rising model (described by Equation (2)). The heat loss, i.e., light energy lost to convert to heat, and heat dissipation during light-to-heat conversion, limits the temperature rising rate, thus induces lower positive temperature-change rate than expected. For negative temperature-change rate, the heat dissipation model described by Equation (6) neglects the contribution of the electrodes to heat dissipation. In the sandwiched PG device, the top and bottom electrodes would enhance the heat dissipation rate, especially for the device with graphene electrode which is known for its superior thermal conductivity,[29] thus induces higher negative temperature-change rate than predicted by the model. According to pyroelectric Equation (1), the current/voltage of PG is proportional to the temperature-change rate, which is inversely proportional to the PVDF thickness. So, for the constructed PG devices, the output voltage/current would rapidly drop as the PVDF thickness increases (Figure 2c). It is also noted that the response time (to reach the voltage peak) is also dependent on the PVDF thickness, as shown in Figure 2c (the inset). It reveals that the responsive time keeps constant for the devices with PVDF thickness in 30–100 μm, but gets larger for those with 200 μm and 500 μm thick PVDF, which can be also attributed to its thickness dependence of heat transfer. In the following, thin PVDF films, 30 μm in thickness, were employed for PG.

2.3. Output Modulations of the PG as a Function of Irradiation Frequency

For bioelectronics for nerve stimulation, it is important to modulate the impulse that flows through the stimulated nerves. The stimulus waveforms, i.e., amplitude, pulse width, monophasic versus biphasic, and the delay between the two phases of the biphasic pulse, would provide the greatest excitability differences for different nerve fibers.[30] For example, the stimulus duration affects the relative selectivity among different diameter nerve fibers. Shorter pulse widths produce a larger threshold difference between different diameter nerve fibers.[31] **Figure 3** shows the modulation of the output voltage waveforms, i.e., pulse amplitude, pulse width, and the accompanied positive and negative pulses and the delay time between them, by adjusting nIR irradiation. When the durations of irradiation "on" and "off" are equal, it can be found that the output voltage

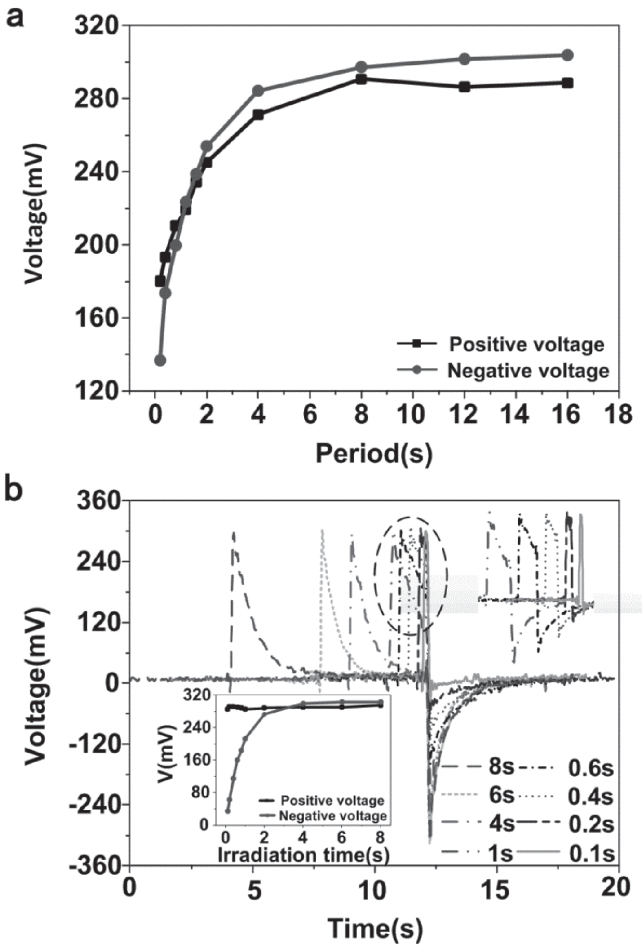

Figure 3. Characterization of the battery-less PG device and its output modulations. a) Positive and negative voltage generated at different periods. b) Modulation of voltage pulse by irradiation time when the nonirradiation time is fixed. (a) and (b) indicate that the pulse width and amplitude can be modulated by the times of irradiation "on" and "off."

is enhanced when the duration prolongs, and finally gets saturated (when 8 s in period, that is 4 s in irradiation "on," as Figure 3a illustrates). It may be attributed to the temperature-change rate of the PG that continuously rises until it reaches saturated value when the irradiation duration prolongs. The voltage for various irradiation periods in Figure 3a is the value when the temperature-change rate of the PG reaches a steady state. Although the initial voltage gets to the same value due to nearly the same temperature-change rate at the time of irradiation "on," drop on output voltage peak at steady state occurs for that with a short time of irradiation "off" (which affects the heat dissipating), as Figure S7a–d (Supporting Information) shows, and the drop gradually decreases when the duration of irradiation "off" prolongs, and finally disappears over 6 s in irradiation "off" time, which indicates that after 6 s for heat dissipating, the heat accumulating in the irradiation "on" duration can be completely dissipated, and the surface temperature of the PG device at the time of next irradiation "on" is completely recovered to room temperature, such as Figure S7e,f (Supporting Information) shows.

When the duration of irradiation "off" is fixed at 6 s, the time of irradiation "on" dependence of output voltage and its waveform are shown in Figure 3b. The pulse width of positive output can be modulated gradually while keeping the same amplitude (the inset in Figure 3b). It clearly indicates that the positive pulse amplitude only depends on the temperature-ascend rate (which gets to maximum at exactly the time of irradiation "on"), which can be modulated by the irradiation intensity (as Figure 2b shows), while its pulse width can be modulated by the duration of irradiation "on." On the other hand, the pulse width of negative output remains the same while its amplitude drops as the decrease of the irradiation time. Compared to waveform of the positive pulse, the contrary behavior of negative pulse can be attributed to the different effects of the device temperature. Shortening irradiation time induces a lower device temperature, which would result in a lower temperature-descend rate at the time of irradiation "off," thus inducing a lower negative pulse amplitude. The negative pulse width is dependent on the duration of heat dissipating, which is roughly independent on the irradiation time. From Equation (3), the positive temperature-change rate at the time of irradiation on is independent on irradiation time. So, the positive temperature-change rates at the time of irradiation on are all the same under different irradiation time. According to Equation (6), the negative temperature-change rate at the time of irradiation off, which indicates the heat dissipation process when nIR off, is proportional to irradiation time (Δt). Longer irradiation time induces larger negative temperature-change rate at the time of irradiation off. The irradiation time dependence of the negative temperature-change rate is measured when the irradiation "off" is fixed at 6 s (Supporting Information, Figure S8). From waveform showed in the inset figure, the negative temperature-change rate at the time of irradiation off decreases when irradiation time is from 1 to 0.1 s. The temperature-change rate waveform agrees with the output voltage waveform (Figure 3b). In addition, the pulse widths of both the positive and negative temperature-change rates rely on the irradiation time, which supplies a possible approach to modulate the output waveform. For example, the pulse width of waveform can be further shortened to milliseconds when the irradiation on/off time is 40 ms/1 s (Supporting Information, Figure S9), which can be used for bioelectronic devices.[32,33] The modulations of positive and negative pulses clearly reveal that we can modulate the waveform of the output pulse by carefully designing the nIR irradiation, which is promising in nerve stimulations.

2.4. PG Lamination for Miniature and Further Output Enhancement

According to Equation (1), to further enhance the output voltage/current of PG, the device area needs to be increased, which induces a large volume and difficulties for implant. In addition, the surface temperature of the PG device would be one of the critical issues to limit its use as an implantable device, due to the potential adverse biological responses. Animal experimental models have been established to investigate the clinical hyperthermia and their biological effects in

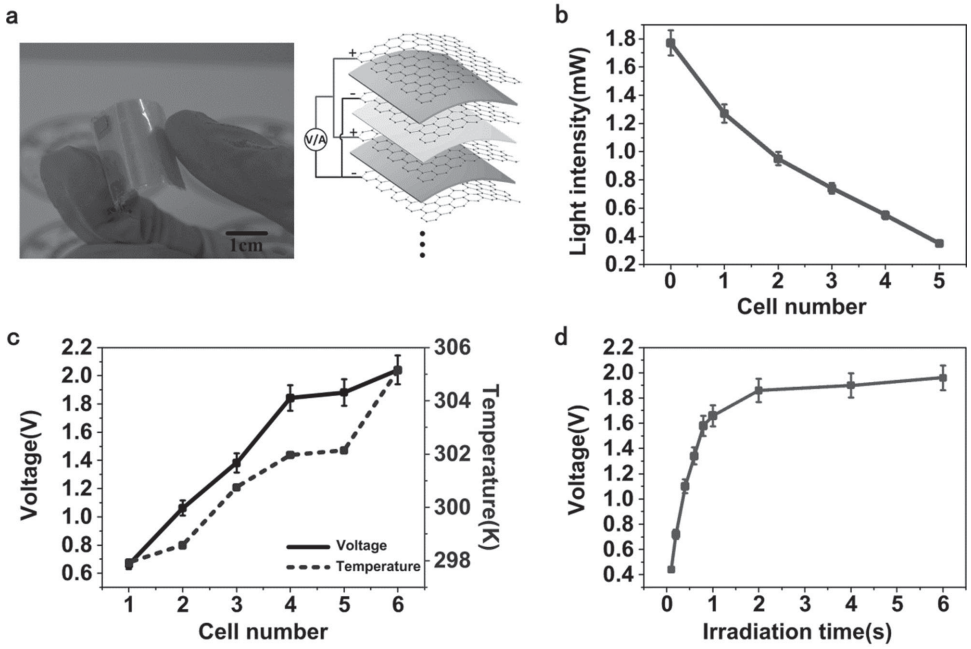

Figure 4. Laminated PG device for miniature and output enhancement. a) Photograph and scheme of flexible laminated PG device. b) Infrared light intensity arriving at each cell of the laminated device. c) Laminated cell number dependence of the open-circuit voltage output and the temperature on the top. d) The irradiation time dependence of the open-circuit voltage.

previous studies, which indicates that the temperatue increases which are insufficient to induce irreversible damage are 10–13 K for bones[34] and 9 K for tissues.[35] In order to improve the output electricity and also meet the requirements of miniature and biocompatibility for temperature increases, several PGs were connected in parallel in a lamination way by utilizing the high transmittance of graphene, whose scheme is shown in **Figure 4**a. Graphene was transferred on both sides of the PVDF films as electrodes. Because of its high transparency of graphene and the well transmittance of thin PVDF film (Supporting Information, Figure S1), it is possible to laminate several graphene–PVDF–graphene sandwiched cells to ensure each cell could get nIR irradiation.

Figure 4b shows the incident light decay by passing through the laminated cells. It reveals that the light intensity decays gradually when the laminated cell number ranges from 1 to 6, and the transmittance of nIR light also decreases accompanied with the increase of cell number (Supporting Information, Figure S10). Figure 4c shows the laminated cell number dependence of the output voltage. The irradiation on and off time is 1 s/4 s. Although the final output is not linearly dependent on the laminated cell number, e.g., the light–current conversion efficiency of the bottom layer of PVDF is about 10% of the top layer of PVDF due to the incident nIR light for each cell gradually decays from the top, by laminating 6 PG cells, the output voltage can be up to 2 V, a great enhancement compared to a single cell. It should be also noted that the temperature of the top cell, which is the highest in the laminated cells, slightly rises as the increase of stacked cell number, which can be attributed to the deterioration of heat dissipation for multicell lamination (Figure 4c). For laminated PG device, the temperature of the top cell is dependent on the cell number (Figure 4c). Due to the excellent transparency of the top and bottom graphene electrodes, as well as the good transparency of thin PVDF film (30 μm) to nIR, for a graphene–PVDF–graphene single cell, the nIR absorption is quite weak, resulting in little temperature rise and weak output voltage/current signals (Supporting Information, Figure S11). For multicell-stacked laminated PG device, because of the introduction of multiinterfaces between cells[36] and increment of effective absorption area, the nIR absorption is greatly enhanced (as Figure 4b shows), which also induces higher temperature than that of single cell. Compared to a single graphene–PVDF–Al cell, by graphene–PVDF–graphene cell lamination, the highest temperature when irradiation is 305 K, only 9 K increase to the base temperature (within the safe temperature range to avoid tissue damage), much lower than that of graphene–PVDF–Al single cell (around 28 K increase to the base temperature), which is favorable and environment-friendly for implants. In addition, although incorporating multiple cells, no obvious changes on the flexibility of laminated PGs were observed compared to the single PG cell (Supporting Information, Figure S12). Mechanical fatigue and durability tests were also conducted (Supporting Information, Figures S13 and S14). The performance of laminated PGs barely deteriorates after over thousands of bending and after working for so long time. But the spatial selectivity of constructed laminated cells is still restricted due to the dimension (20 mm × 20 mm × 0.2 mm), which limits its applications for implantable medical devices.[37,38] The further reduction of the device volume is still needed, which may be achieved by increasing the lamination layers, as well as adopting materials with larger pyroelectric coefficient.

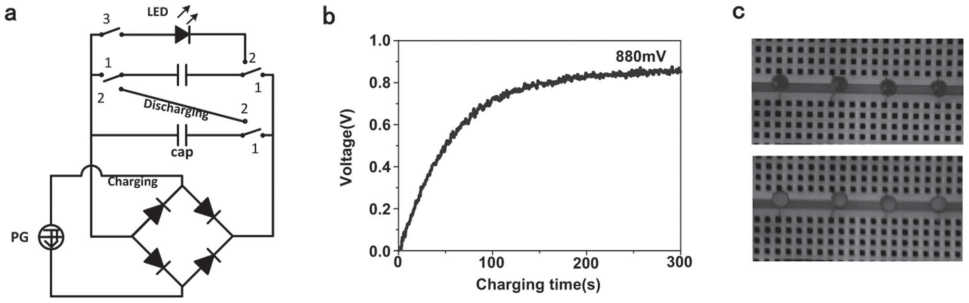

Figure 5. Wireless powering for electronics by the developed battery-less device. a) Scheme of the rectifying circuit. b) Voltage obtained by a capacitor when being charged by the battery-less device. c) Snapshots of LEDs driving by the stored charges.

2.5. Wireless Powering for Electronics

To illustrate the wireless-powering ability of the developed battery-less device, a current rectification and energy storage system was implemented using a commercial full-wave bridge rectifier (**Figure 5**a). The generated electricity was stored consecutively by connecting two 10 μF capacitors in parallel. The voltage outputs of the PG before and after rectification (Supporting Information, Figure S15) clearly demonstrate full-wave rectification. The entire charging process was recorded by monitoring the voltage across a capacitor, as presented in Figure 5b. As the charging process continued, the voltage of each capacitor was saturated at around 0.88 V, which was lower than the output voltage of the PG, possibly due to voltage drop consumed at the rectifying diodes and/or the leakage of the capacitors.[39] Then, by connecting the two charged capacitors in series, the total output voltage reached $V_{tot} = 0.88 \times 2 = 1.76$ V, which can be used to drive a LED with a turn-on voltage of ≈1.6 V. By using this voltage amplification technique, we successfully powered four commercial LEDs by a fast discharge of the stored charges in fourteen capacitors, as shown in Figure 5c.

The total electrical energy stored by the capacitor can be calculated as $W_{stored} = C\ U^2 n/2 = 54.2$ μJ, where C is the capacitance of a single capacitor, U is voltage across the capacitor, and n is the number of capacitors. The power generated by the PG may not be sufficient to continuously drive the operation of a device, but an accumulation of charges generated over a period of time is sufficient to drive the device for a fraction of a second. This can be of practical use for devices that have standby and active modes, such as glucose sensors and blood pressure sensors for health monitoring that are only required to be in active mode periodically.[39,40]

2.6. Remote Manipulation for Nerve Stimulations

The real-time functional electrical stimulation (FES) of nerves and neurons by the PG has potential biomedical application for the repair of biological neural network[41] and the wireless-powering heart pacemaker.[42] Due to the excellent biocompatibilities of the adopted PVDF and graphene and its modulative output electrical pulse of the device, the battery-less device is suitable for implantable bioelectronics. Here, we employed the laminated PG device (Figure 4a) as an implantable stimulator for real-time functional electrical stimulation of a sciatic nerve of a frog and a rat heart, by a remote control by nIR irradiation. For a frog's sciatic nerve, stimulation by a voltage of over 50 mV at 1 Hz is necessary for innervation. When the input voltage is beyond the threshold voltage of the resting potential, a contraction of muscle would be induced by opening the valve of the action potential.[41,43] The open-circuit voltage of the PG (Figure 4c) is enough to achieve functional electrical stimulation. The scheme of experimental set-up is shown in **Figure 6**a. The positive and negative terminals of the PG were connected to the white corded sciatic nerve from an interceptive hind limb of a frog. Through the stimulation by the output voltage pulse of the laminated device, muscle contraction was clearly observed through the tension response in Figure 6b. The stimulation video can be found in Video file 1 (Supporting Information).

Figure 6c provides the scheme of a remote-controllable cardiac stimulator composed by the flexible battery-less device. The implantable flexible cardiac stimulator was directly linked to stimulation electrodes to provide electrical stimuli to the heart of an anesthetized rat. The simultaneously recorded electrocardiogram (ECG) in a normal rat heart before the stimulation is shown in Figure S16 (Supporting Information). Figure 6d shows the laminated PGs were implanted subcutaneously in a living rat for heart stimulation by electrical pulse generated by the developed laminated device when nIR laser irradiated the rat periodically from outside. To reach the required electric energy to trigger the action potential and contraction of the heart, an infrared light with larger light intensity was employed. When the rat was irradiated cyclically by infrared light, the corresponding spike peaks were observed on the natural heartbeat of the rat in the ECG, as visualized in Figure 6e. When the stimulated current amplitude output by the battery-less device updates, corresponding ECG peaks were observed (see Supporting Information, Video file 2). This result shows that the proposed PGs device has potential biomedical use for the normalization of cardiac function. The remote-controllable electrical stimulation of the heart by a battery-less device would find great applications in the developments of self-powered artificial heart pacemaker.

3. Conclusion

A nIR-driven wireless-powering device (PG) composed of pyroelectric PVDF microbelts has been developed. By controllable nIR flashing remotely, the wireless-powering device can absorb

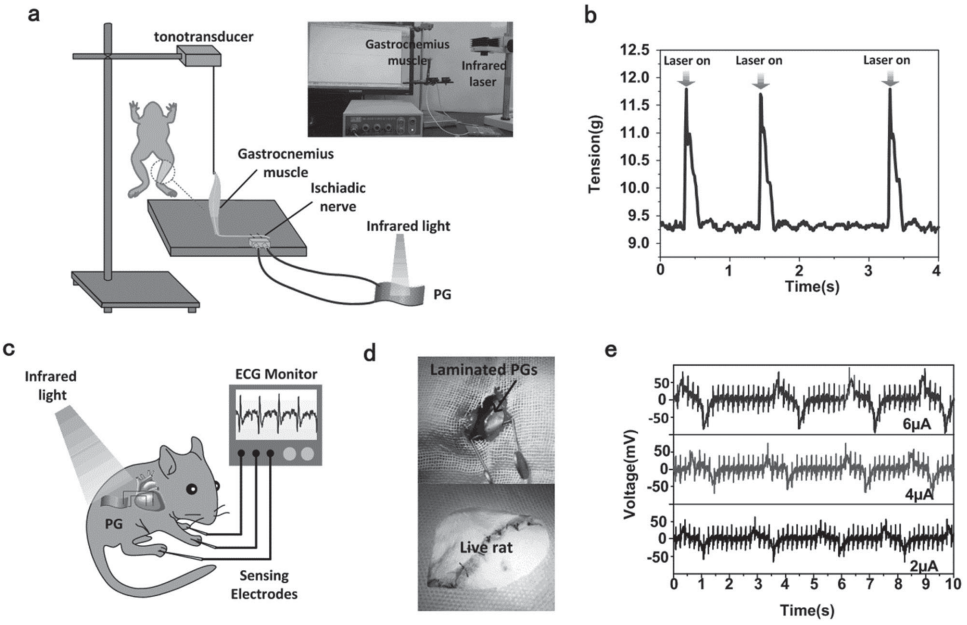

Figure 6. Remote-manipulative electrical stimulation by the developed battery-less device. a,b) Stimulation of a sciatic nerve of a frog. a) Experimental set-up for real-time functional electrical stimulation. b) Tension profile during stimulation by controllable irradiating the device. c–e) Heart stimulation on a live rat. c) Scheme of the stimulation by the electrical pulse generated by laminated PG device, and d) the laminated PG device was implanted subcutaneously in rat. e) Recorded real-time ECG in a live rat during heart stimulation by electrical pulse generated by the battery-less device. The remarkable artificial peaks on the ECG arise from the stimuli clearly showing the validation of the remote-manipulative stimulation.

light and generate voltage/current pulse, which is promising for biological nerve stimulation or batteries charging. It is observed that the output voltage/current is determined by irradiation light intensity and the thickness of the adopted PVDF; the short-circuit current of the PG is gradually enhanced when the irradiation light intensity elevated; the voltage drops as the increase of PVDF thickness. The output voltage waveforms, i.e., pulse amplitude, pulse width, and the accompanied positive and negative pulses and the delay time between them, can be modulated by adjusting nIR irradiation, which is important to construct bioelectronics modulating the impulse that flows through the stimulated nerves. Furthermore, in order to enhance its electric properties while reducing the device temperature to avoid damage to intervening and surrounding normal tissue, a compact laminated wireless-power device, in which each cell is composed of graphene–PVDF–graphene sandwich, has been developed. The constructed laminated wireless-powering device, which is compact (20 mm × 20 mm × 0.2 mm) and flexible, can generate voltage and current up to 2 V and 200 nA, in response to nIR remote irradiation. The generated electric energy can be effectively stored to light up an array of commercial LED, and also can be directly applied for nerve stimulation, such as sciatic nerve of a frog, and the heart of a live rat, indicating that the proposed battery-less device can be candidate for bioelectronics.

4. Experimental Section

Fabrication and Characterization of the PG Device: A single-cell PG device was fabricated by coating electrode material on both sides of PVDF film (20 mm × 5 mm, in various thicknesses). Al electrode with thickness 100 nm was deposited on the PG by magnetron sputtering. The infrared laser (λ = 808 nm, $S_{light\ spot}$ = 5 mm × 2 mm, 2 W cm^{-2} in light density)) was employed. The infrared light was illuminated on the top of device periodically by a controlled shutter to offer controllable irradiation. The thermal infrared imager (SC7300M, FLIR Systems AB) was used to record the temperature of the PG. The temperature was measured from the whole sample, and its distribution was shown in Figure S17 (Supporting Information). As the spot size is much smaller than that of PG, the temperature distribution cannot cover the whole device. The temperature values we used were the average values of the hot regions. The generated voltage and current pulse were measured by using a digital phosphor oscilloscope (Tektronix DPO 3034) and a semiconductor characterization system (KEITHLEY 4200).

Fabrication of Graphene Electrode and Laminated PG Device: The graphene was synthesized according to the chemical vapor deposition (CVD) method. The Raman spectrum of the graphene film used in this study (Supporting Information, Figure S18) indicates a single-layer graphene sheet with relatively low defect density. Then the graphene film was transferred on the one side of 30 μm thick PVDF film (20 mm × 5 mm) from the Cu foil by the typical transfer method using poly(methylmethacrylate) (PMMA). The laminated PG device was fabricated by laminating various PG cells with graphene electrode on both sides of PVDF film (20 mm × 20 mm) in parallel separated by some insulating layers.

The Real-Time Functional Electrical Stimulation (FES) Experiments: All animal experiments were performed in compliance with the Xi'an Jiaotong University Health Science Center and the First Affiliated Hospital of Xi'an Jiaotong University. The positive and negative terminals of the laminated PGs were connected to the binding post of the stimulating electrode attached to the white corded sciatic nerve from an interceptive hind limb of a frog. In the experiment, the nerve and gastrocnemius muscle were kept wet by Ringers solution for amphibians. The nerve stimulation experiments were performed generally when dissection after 10 min. A rat was placed under anesthesia with chloral hydrate (1%), and an incision was made on precordium of the rat. Three terminals were pinned to the rodent, on the left posterior leg and both

anterior legs, to monitor its ECG. The flexible laminated PGs implanted subcutaneously in the living rat were linked to stimulation electrodes to make artificial heartbeat of the live rat using generated electric output from the device. In order to avoid the foreign body fibrous capsule affect the sensitivity of the device, the laminated PGs were capsulated by thin PDMS film (about 1 μm thickness). In animal experiments, six frogs and six rats had been used respectively in the real-time FES experiments for electrical stimulation of the sciatic nerve of the frog and the rat heart. And the rat we used in this experiment was anesthetized; the experiments performed on arrhythmic rats and the long-term effect of laminated PGs on the heart rate of arrhythmic rats will conduct in future work.

Supporting Information

Supporting Information is available from the Wiley Online Library or from the author.

Acknowledgements

The authors gratefully appreciate the financial supports by the National Natural Science Foundation of China (Grant Nos. 91323303, 51305337, 51275400). It is a great pleasure to thank S. Wang from the First Affiliated Hospital of Xi'an Jiaotong University, for many useful discussions and related experiments. The authors also acknowledge J. Zhao and X. Sun in Xi'an Jiaotong University Health Science Center for their assistance on the animal experiments.

Received: July 6, 2015
Revised: September 5, 2015
Published online: October 29, 2015

[1] K. Famm, B. Litt, K. J. Tracey, E. S. Boyden, M. Slaoui, *Nature* **2013**, *496*, 159.
[2] S. Reardon, *Nature* **2014**, *511*, 18.
[3] C. Dagdeviren, B. D. Yang, Y. Su, P. L. Tran, P. Joe, E. Anderson, J. Xia, V. Doraiswamy, B. Dehdashti, X. Feng, B. Lu, R. Poston, Z. Khalpey, R. Ghaffari, Y. Huang, M. J. Slepian, J. A. Rogers, *Proc. Natl. Acad. Sci. USA* **2014**, *111*, 1927.
[4] H. Mei, P. P. Irazoqui, *Nat. Biotech.* **2014**, *32*, 1008.
[5] M. D. Tang-Schomer, X. Hu, M. Hronik-Tupaj, L. W. Tien, M. J. Whalen, F. G. Omenetto, D. L. Kaplan, *Adv. Funct. Mater.* **2014**, *24*, 1938.
[6] I. Hochmair, *Nat. Med.* **2013**, *19*, 1240.
[7] Y. Aponte, D. Atasoy, S. M. Sternson, *Nat. Neurosci.* **2011**, *14*, 351.
[8] L. W. Diao, J. Zheng, X. D. Pan, W. Zhang, L. F. Wang, L. Z. Sun, *J. Thora. Dis.* **2014**, *6*, 1300.
[9] M. A. Karami, D. J. Inman, *Appl. Phys. Lett.* **2012**, *100*, 042901.
[10] L. Halámková, J. Halámek, V. Bocharova, A. Szczupak, L. Alfonta, E. Katz, *J. Am. Chem. Soc.* **2012**, *134*, 5040.
[11] P. P. Mercier, A. C. Lysaght, S. Bandyopadhyay, A. P. Chandrakasan, K. M. Stankovic, *Nat. Biotech.* **2012**, *30*, 1240.
[12] N. M. Neihart, R. R. Harrison, *IEEE Trans. Biomed. Eng.* **2005**, *52*, 1950.
[13] J. S. Ho, A. J. Yeh, E. Neofytou, S. Kim, Y. Tanabe, B. Patlolla, R. E. Beygui, A. S. Y. Poon, *Proc. Natl. Acad. Sci. USA* **2014**, *111*, 7974.
[14] E. Y. Chow, Y. Ouyang, B. Beier, W. J. Chappell, P. P. Irazoqui, *IEEE Trans. Microwave Theory Tech.* **2009**, *57*, 2523.
[15] D. J. Yeager, J. Holleman, R. Prasad, J. R. Smith, B. P. Otis, *IEEE Trans. Biomed. Circuits Sys.* **2009**, *3*, 379.
[16] W. J. Heetderks, *IEEE Trans. Biomed. Eng.* **1988**, *35*, 323.
[17] S. S. Cui, D. Y. Yin, Y. Q. Chen, Y. F. Di, H. Y. Chen, Y. X. Ma, S. Achilefu, Y. Q. Gu, *ACS Nano* **2013**, *7*, 676.
[18] E. Vinck, B. Cagnie, P. Coorevits, G. Vanderstraeten, D. Cambier, *Lasers Med. Sci.* **2006**, *21*, 11.
[19] R. Weissleder, *Nat. Biotech.* **2001**, *19*, 316.
[20] D. Lingam, A. R. Parikh, J. Huang, A. Jain, M. Minary-Jolandan, *Int. J. Smart Nano Mater.* **2013**, *4*, 229.
[21] C. L. Sun, J. Shi, D. J. Bayerl, X. D. Wang, *Energy Environ. Sci.* **2011**, *4*, 4508.
[22] Z. Li, X. Zhang, G. Li, *Phys. Chem. Chem. Phys.* **2014**, *16*, 5475.
[23] E. S. Kulkarni, S. P. Heussler, A. V. Stier, I. Martin-Fernandez, H. Andersen, C. -T. Toh, B. Özyilmaz. *Adv. Opt. Mater.* **2015**, *3*, 34.
[24] D. Choi, M.-Y. Choi, W. M. Choi, H.-J. Shin, H.-K. Park, J.-S. Seo, J. Park, S.-M. Yoon, S. J. Chae, Y. H. Lee, S.-W. Kim, J.-Y. Choi, S. Y. Lee, J. M. Kim, *Adv. Mater.* **2010**, *22*, 2187.
[25] R. W. Whatmore, *Rep. Prog. Phys.* **1986**, *49*, 1335.
[26] C. R. Bowen, H. A. Kim, P. M. Weaver, S. Dunn, *Energy Environ. Sci.* **2014**, *7*, 25.
[27] Y. Yang, J. H. Jung, B. K. Yun, F. Zhang, K. C. Pradel, W. X. Guo, Z. L. Wang, *Adv. Mater.* **2012**, *24*, 5357.
[28] C. R. Bowen, J. Taylor, E. L. Boulbar, D. Zabek, V. Y. Topolov, *Mater. Lett.* **2015**, *138*, 243.
[29] A. A. Balandin, S. Ghosh, W. Z. Bao, I. Calizo, D. Teweldebrhan, F. Miao, C. N. Lau, *Nano Lett.* **2008**, *8*, 902.
[30] P. H. Gorman, J. T. Mortimer, *IEEE Trans. Biomed. Eng.* **1983**, *30*, 407.
[31] W. M. Gill, J. T. Mortimer, *IEEE Eng. Med. Biol.* **1995**, *95*, 0739.
[32] C. C. McIntyre, W. M. Grill, *J. Neurophysiol.* **2002**, *88*, 1592.
[33] J. W. Leem, E. S. Park, K. S. Paik, *Neurosci. Lett.* **1995**, *192*, 197.
[34] A. R. Eriksson, T. Albrektsson, *J. Prosthetic Dent.* **1983**, *50*, 101.
[35] L. R. Hirsch, R. J. Stafford, J. A. Bankson, S. R. Sershen, B. Rivera, R. E. Price, J. D. Hazle, N. J. Halas, J. L. West, *Proc. Natl. Acad. Sci. USA* **2003**, *100*, 13549.
[36] Q. Q. Miao, L. Q. Wu, J. N. Cui, M. D. Huang, T. L. Ma, *Adv. Mater.* **2011**, *23*, 2764.
[37] H. Mei, P. P. Irazoqui, *Nat. Biotechnol.* **2014**, *32*, 1008.
[38] J. S. Ho, A. J. Yeh, E. Neofytou, S. Kim, Y. Tanabe, B. Patlolla, R. E. Beygui, A. S. Y. Poon, *Proc. Natl. Acad. Sci. USA* **2014**, *111*, 7974.
[39] S. Xu, B. J. Hansen, Z. L. Wang, *Nat. Commun.* **2010**, *1*, 1.
[40] Z. L. Wang, *Adv. Mater.* **2012**, *24*, 280.
[41] L. Gu, N. Y. Cui, L. Cheng, Q. Xu, S. Bai, M. M. Yuan, W. W. Wu, J. M. Liu, Y. Zhao, F. Ma, Y. Qin, Z. L. Wang, *Nano Lett.* **2013**, *13*, 91.
[42] G.-T. Hwang, H. Park, J.-H. Lee, S. Oh, K.-I. Park, M. Byun, H. Park, G. Ahn, C. K. Jeong, K. No, H. Kwon, S.-G. Lee, B. Joung, K. J. Lee, *Adv. Mater.* **2014**, *26*, 4880.
[43] S. A. Raymond, *J. Physiol.* **1979**, *290*, 273.